The evolution of the moraine complex in the Fiescher Valley (Berner Alps, Switzerland) in the light of Schmidt-hammer exposure-age dating and sedimentological analysis

Dawid Siemek[1], Magdalena Jasionek[2], Piotr Kłapyta[3], Patryk Wacławczyk[4]

[1] Jagiellonian University, Faculty of Geography and Geology, Krakow, Poland, e-mail: dawid.siemek@doctoral.uj.edu.pl (corresponding author), ORCID ID: 0009-0006-2010-5952

[2] Jagiellonian University, Faculty of Geography and Geology, Krakow, Poland, e-mail: magdalena.jasionek@student.uj.edu.pl, ORCID ID: 0000-0002-9584-0269

[3] Jagiellonian University, Faculty of Geography and Geology, Krakow, Poland, e-mail: piotr.klapyta@uj.edu.pl, ORCID ID: 0000-0001-6853-4074

[4] Jagiellonian University, Faculty of Geography and Geology, Krakow, Poland, e-mail: patryk.waclawczyk@doctoral.uj.edu.pl, ORCID ID: 0000-0003-3142-9400

Abstract: The sediment-landform assemblages preserved in many alpine valleys record glacier fluctuations during the latest Pleistocene and Holocene, encompassing the moraines formed during the Egesen stadial as well as Early Holocene and Neoglacial advances. This paper is concerned with the moraine evolution in the Fiescher Valley, a relatively large glaciated alpine valley system in the Berner Alps which hosts the fourth-largest glacier in the Alps. A geomorphological and sedimentological analysis supplied with Schmidt-hammer exposure age-dating was used on the preserved moraine sequence along a 7-kilometre section of the valley. Calibrated Schmidt-hammer weathering results provide evidence of the multiphase glacier readvances of the Fischer glacier during the Younger Dryas and Early Holocene. The exposure age of Holocene boulders strongly differs with the time of moraine formation as the result of the incorporation of more weathered boulders originated by earlier glacier fluctuactions and rockfall activity. We thus infer that the previously formed Middle Holocene moraines were overridden by the much more extensive LIA advance. Sediment transport pathways in the Fiescher Valley were dominated by subglacial active erosion and transportation pathways of massive crystalline rocks, discernible via the large proportion of subrounded and subangular clasts. We found that significant and multiple glacial remodelling is arguably the most efficient way to reduce the initial platy shape of granitic and gneiss clasts but a dependence between clast form and roundness with distance is hardly visible.

Keywords: Berner Alps, Fiescher Valley, Schmidt-hammer exposure age-dating, clast shape analysis, calibration curve

INTRODUCTION

Modern Alpine glaciers experience rapid geomorphological and sedimentological changes related to the accelerating loss of mass due to ongoing warming (Avian et al. 2018, Le Heron et al. 2021, Rounce et al. 2023). Due to the competing influence of subglacial, ice-marginal and proglacial processes, rapid lateral and vertical changes in sediment lithofacies are reported from recently exposed Alpine glacial environments (Le Heron et al. 2021). The formation of moraines and the

sedimentological characteristics of glacial deposits in alpine catchments have recently been the subject of detailed geomorphological studies (e.g. Schindelwig et al. 2012, Reznichenko et al. 2016, Braumann et al. 2020). These studies drew attention to the geomorphological record of ice-marginal landforms in relatively small glaciated valley systems (*sensu* Benn et al. 2003), which are regarded as the key localities for tracing the impact of climate and topography on glacier development (Lukas & Benn 2006, Zasadni 2007, Schindelwig et al. 2012, Schimmelpfennig et al. 2021). Small glaciated catchments are also priority sites for the development of glacial chronology utilized by both relative dating methods (Matthews & Winkler 2022) and cosmogenic surface exposure dating (Pallàs et al. 2010, Lukas et al. 2013, Zasadni & Kłapyta 2016, Longhi & Guglielmin 2020 2021, Kłapyta et al. 2021, Scapozza et al. 2021). In contrast, in much larger glacial systems (>20 km^2), due to a longer glacier response time and the effect of erosional censoring of moraines, the record of climatic oscillations in glacial landforms and sediments may be significantly limited (Kirkbride & Winkler 2012, Schindelwig et al. 2012).

The Swiss Alps are one of the main European areas where Late Glacial and Holocene glacial chronologies have been developed based on cosmogenic surface exposure dating (Hormes et al. 2001, Joerin et al. 2006, Ivy-Ochs 2015, Braumann et al. 2020, Ivy-Ochs et al. 2023). The Berner Alps host the largest present-day alpine glaciers including Great Aletsch Glacier (87 km^2 area), and Fiescher Glacier (33 km^2 area) (World Glacier Inventory). In this area the ^{10}Be-based moraine chronology has been elaborated for the Great Aletsch (Kelly et al. 2004, Schindelwig et al. 2012) and Unnerbäch glaciers (Schindelwig et al. 2012), where the youngest, well-preserved Late Glacial moraines stabilized during the Younger Dryas or Early Holocene, between 12.7 ka ±1.1 ka to 10.7 ka ±1.3 ka (Scotti et al. 2017). A similar age, 11.1 ka ±0.7 ka, was determined for the stabilization of moraines in the neighboring Grimsel area (Ivy-Ochs et al. 1996) as well as in the other Alpine regions (see e.g. Ivy-Ochs et al. 1996, 2006, 2022, Baroni et al. 2021). In contrast, the moraine deposition history of the fourth largest alpine glacier in the Fiescher Valley has been largely undetected up to now.

In parallel with absolute dating methods, the low-cost and portable Schmidt-hammer (SH) technique has recently been used in the Alps to reconstruct the history of deglaciation (Böhlert et al. 2011, Scotti et al. 2017, Longhi & Guglielmin 2020, 2021, Scapozza et al. 2021). The SH rebound values (*R*-values) provide a quantitative measure of rock hardness which is influenced by the duration of rock surface exposure to weathering. Therefore, it could be used to determine relative and absolute age, where *R*-values are calibrated with surfaces of known age (Schmidt-hammer exposure-age dating, SHED) (Matthews & Winkler 2022). The recent applications of SHED in the Italian and Swiss Alps (Scotti et al. 2017, Longhi & Guglielmin 2020, 2021, Scappoza 2021) indicate the potential for dating moraines of small glaciers, where 4 to 7 glacial stages were distinguished between Egesen I (13.1 ka ±1.1 ka) and the Little Ice Age (LIA).

The moraine deposition history can be further elucidated through the analysis of clast morphology, including clast shape and roundness (Benn and Balantyne 1994, Lukas et al. 2013). This approach has been used in the Alps for the determination of sediment composition and transport pathways for a small cirque glacier (Roberson 2008), as well as the formation of sediments within the Haut Glacier d'Arolla moraines (Hambrey et al. 2002, Goodsell et al. 2005). The mutual combination of the Schmidt hammer and clast morphology analysis has only been proposed in a few works aimed at analysing the formation of periglacial landforms (Reznichenko et al. 2016, Winkler et al. 2020) or distinguishing glacial from landslide deposits (Kłapyta 2020). By combining both methods, it is possible to infer a correlation between the clasts' shape and the age of moraines, providing insights into the dynamics of glacial processes during time.

In the Fiescher Valley, the currently retreating glacier snout has recently exposed sediments that can be compared with earlier advances of unknown age. The main aim of this study is to reconstruct the evolution of the moraine sequence in the Fiescher Valley based on the results of geomorphological mapping, SH relative age dating and

sedimentological analysis. An attempt was made to determine the impact of transport length and surface weathering on the formation and preservation of moraines. Additional objectives are: (i) construction of a local age calibration curve based on the Schmidt-hammer exposure-age dating, (ii) determination of transport and deposition history of moraine clasts, (iii) correlation of moraine clast morphology and the composition of fine-grained sediments with the SH weathering index.

STUDY AREA

The Fiescher Valley (German: Fiescher Thal) (33,06 km² area) is a right-hand tributary of the Rhône Valley located on the southern slope of the Berner Alps in Switzerland (Fig. 1). The mountain ridges surrounding the 20-km-long Fiescher Valley rise between 3,000 to 4,000 m a.s.l., reaching a maximum elevation of 4,274 m a.s.l. at the top of Finsteraarhorn (Fig. 1B).
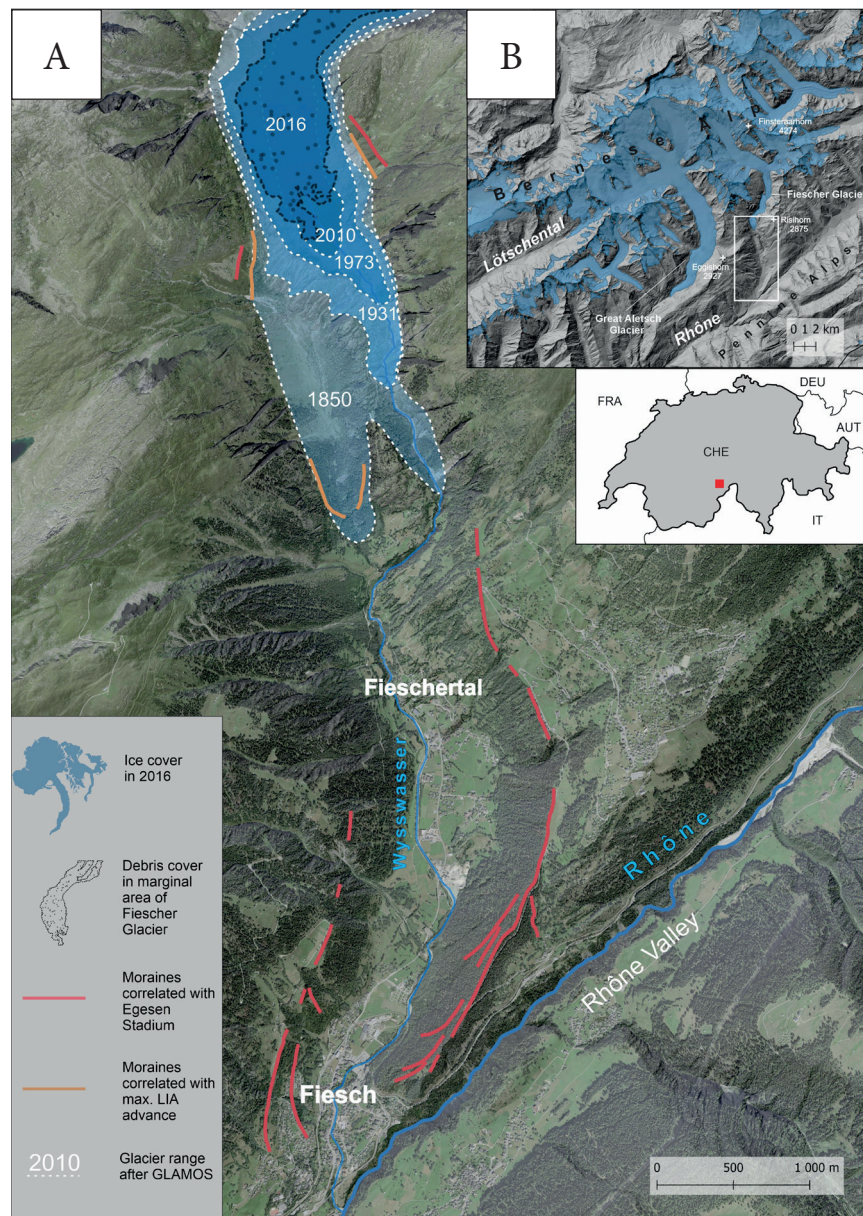

Fig. 1. Location of the study area: A) middle and lower sections of the Fiescher Valley with marked moraines correlated with Egesen stadial and maximum LIA extent (ca. 1850). Extent of moraines after geological map of Switzerland (Federal Office of Topography Swisstopo 2024a) and glacier range after Glacier Monitoring in Switzerland GLAMOS (n.d.); B) Fiescher Valley against the recent glacier extent in the Berner Alps

It is a present-day glaciated high-alpine valley occupied by the fourth largest valley glacier in the Alps, the Fiescher Glacier. In 2017, the Fiescher Glacier was 14.5 km long and covered an area of 29.7 km^2. Its average thickness was 117 m (with a maximum of 437 m), which translated into a total volume of 3.48 km^3 of ice (Glacier Monitoring in Switzerland GLAMOS n.d.). The Fiescher Glacier experienced an intense recession, between 1891 and 2020 when the glacier's snout retreated by 1.6 km, which is about 1 km during 1973–2020 CE (Glacier Monitoring in Switzerland GLAMOS n.d.). In 1973 the equilibrium line altitude (ELA) of the Fiescher Glacier was situated at 2,900–2,950 m a.s.l. (Müller et al. 1976) and the glacier terminated at an altitude of 1,655 m a.s.l. Currently, the frontal part of the glacier is located at an altitude of approx. 1,700 m a.s.l. and is almost entirely covered with supraglacial debris. Below the glacier's snout, a 7 km long section of the valley hosts a well-preserved sequence of moraine ridges which have been deposited since the Egesen stadial, corresponding to the glacier advance during the Younger Dryas (12.9–11.5 ka) (Steck 2011). The investigated moraine deposits have been preserved throughout the longitudinal profile of the valley between 1,200 and 1,700 m a.s.l. Particularly distinct are the moraines associated with the Egesen stadial, maximum Little Ice Age advance (ca. AD 1850) and glacier front mapped in 2016 CE (Fig. 1A).

The bedrock in the study area is mainly composed of crystalline rocks of the Aar Massif, bordering to the south by sedimentary rocks of the Gotthard Massif (Labhart 1977, Steck 2011). The ridges surrounding the upper part of the Fiescher Valley are built with Permian amphibolites and granites while in lower valley section by pre-Variscan and Variscan augen gneisses and orthogneisses. Moraines are composed of clast of predominate crystalline lithology (granites, orthogneisses, augen gneisses and amphibolites) (Steck 2011, Federal Office of Topography Swisstopo 2024a).

The mean annual temperature at the Ulrichen meteorological station (1,380 m a.s.l., ca. 12 km south of the study area) for the period 1991–2020 was 4.2°C (Federal Office for Meteorology and Climatology MeteoSwiss n.d.). The mean July temperature is 14.6°C whereas the January is –7.2°C. The study area receives 1,180 mm of annual precipitation mainly during the summer season. The climatic conditions in the glacierized part of the valley can be described using data from the Jungfraujoch station (3,571 m a.s.l.), where the average annual temperature for the period 1991–2020 was –6.7°C and average July and January temperatures were 0.4°C and –12.5°C, respectively. A statistically significant increase in mean temperatures, both annual and for individual months, of about 0.2°C/10 years is observed in the study area (Federal Office for Meteorology and Climatology MeteoSwiss n.d.).

MATERIALS AND METHODS

Geomorphological mapping

The geomorphological mapping was performed in the field in July 2022 with the support of available topographical and geological maps: Geological Atlas of Switzerland at a scale of 1:25,000 (Federal Office of Topography Swisstopo 2024a) and National Map at a scale of 1:25,000 (Federal Office of Topography Swisstopo 2024b). Additionally, a high-resolution Swiss ALTI3D digital terrain model (Federal Office of Topography Swisstopo 2024c) with a resolution of 2 m and an accuracy of 0.3 m was used to construct the geomorphological map in ArcMap 10.7.1. The mapping was focused on the identification of glacial landforms (moraines and till drift limits) as well as glacially scoured bedrock. Three morphostratigraphic units were distinguished in the study area: (1) the most extensive and the oldest Egesen stadial moraines (Steck 2011), present in the lower section of the valley, (2) Neoglacial moraines with the maximum extent during the 1850 CE, and (3) the most recent recessional moraines within the range of the glacier extents in 1973, 2010 and 2016 CE. The position of the previously mapped ice margins during 1931, 1973, 2010 and 2016 CE (Glacier Monitoring in Switzerland GLAMOS n.d.). were identified in the field. Glacier dynamic is also marked by numerous ice-moulded surfaces, which were also mapped during fieldwork.

Schmidt-hammer rebound test

The Schmidt-hammer method (SH) is widely used in alpine environments as a tool for the non-destructive determination of rock surface

weathering and its relative age. The rebound values (R-values) come from measuring the distance of the spring rebound while pressing the hammer to the rock surface (Shakesby et al. 2006). R-values correspond to the hardness of the rock surface and its relative age, which is most often a function of the time of its exposure to weathering (Goudie 2006, Shakesby et al. 2006, Kłapyta 2013). Therefore, the SH weathering index can be used to support morphostratigraphic analysis and history of rock surface weathering (Placek & Migoń 2005, Kłapyta 2012). In the study, a BN-type Schmidt hammer with an impact energy of 2.207 Nm (Silver Schmidt) was used, applying standard procedures (Matthews & Owen 2010, Viles et al. 2011). Measurement sites were placed at morphologically stable moraine ridges and glacial polishes. In each moraine unit, three to nine sites were selected (Fr-1-18, Fig. 2A, C). At each site, 30 readings were taken from 2–5 boulders, giving a total of 60–150 individual measurements (Kłapyta 2013). At glacial polishes 50 to 100 readings were recorded. Flat rock surfaces free of bulges, cracks and lichens were preferred. The measurements were performed in dry conditions to avoid the moisture effect (Sumner & Nel 2002). Large morainic boulders (>1 m) made of massive, homogenous lithology (mainly granites, orthogneisses and augen gneisses) were selected. Measurements from glacial polishes were performed on the bedrock built with orthogneisses, augen gneisses, amphibolites and migmatites. To avoid the error associated with measuring the surface repeatedly abraded by the glacier, the combined R-values were presented separately for boulders and glacially moulded bedrock. The overall mean from each sample was given with a 95% confidence interval. The significance of the relationship was tested using a t-test with a P level of 0.05. A list of SH locations along with additional information is presented in Table 1.

The Schmidt-hammer age calibration curve

The Schmidt-hammer age calibration curve (Matthews & Winkler 2022) was constructed taking the linear relationship between the average R-values of the youngest (Fr-18) and the oldest (Fr-1) SH sites. The Fr-18 site represents fresh glacier deposits exposed after 2016, thus the age of

the control point is assumed to be 6 years. The oldest control point represents the latero-frontal moraine site (Fr-1) which is attributed to the outermost moraine of the Egesen stadial (Steck 2011). Due to the lack of absolute dating of moraines in the Fiescher Valley, the age of the maximal Egesen advance was adopted from [10]Be dated sites at the neighboring Great Aletsch Glacier (site VBA-8, Schindelwig et al. 2012) and Unnerbäch Glacier (site VBA-23, Schindelwig et al. 2012), where the maximal Egesen stadial moraines were dated at 13.2 ka ±0.6 ka and 11.4 ka ±0.8 ka, respectively. The external lines were given by adding the R-values 95% confidence intervals calculated by the main equation. Given two additional equations, every site's minimum and maximum age was calculated. In this way, the potential dating error was widened while obtaining more reliable results (Tomkins et al. 2018a, Matthews & Winkler 2022).

Sedimentological analysis

To characterize the textural properties of glacial sediments and glacial debris transport pathways, clast morphology analysis (shape and roundness) was carried out according to Lukas et al. (2013). The clast morphology measurements were performed at 12 sites, giving a total of 600 individual measurements (fr-1-12, Fig. 2A, B). At each site, three axes (a – longest, b – medium, c – shortest) were measured for 50 pebble gravel clasts using a steel ruler (Zingg 1935, Ballantyne 1982). The visual degree of rounding was determined on a modified Powers (1953) scale and were expressed as the RA ratio (the percentage of angular and very angular clasts in any sample) and the RWR ratio (the percentage of rounded to well-rounded clasts). The clast shape was quantified using the C_{40} index (the percentage of clasts with axial ratio c/a <0.4). Transportation and depositional clast histories were determined using covariance plots of RA-C_{40} (Benn & Ballantyne 1994, Lukas et al. 2013) and related to glacial debris transport pathways for massive low anisotropy (Type 1 RA-C_{40} covariance plot, Lukas et al. 2013). Due to terrain limitations that prevented in situ measurements of talus and alluvial debris, data obtained from similar lithologies were compiled from the synthesis of Lukas et al. (2013) and added to the covariance plots.
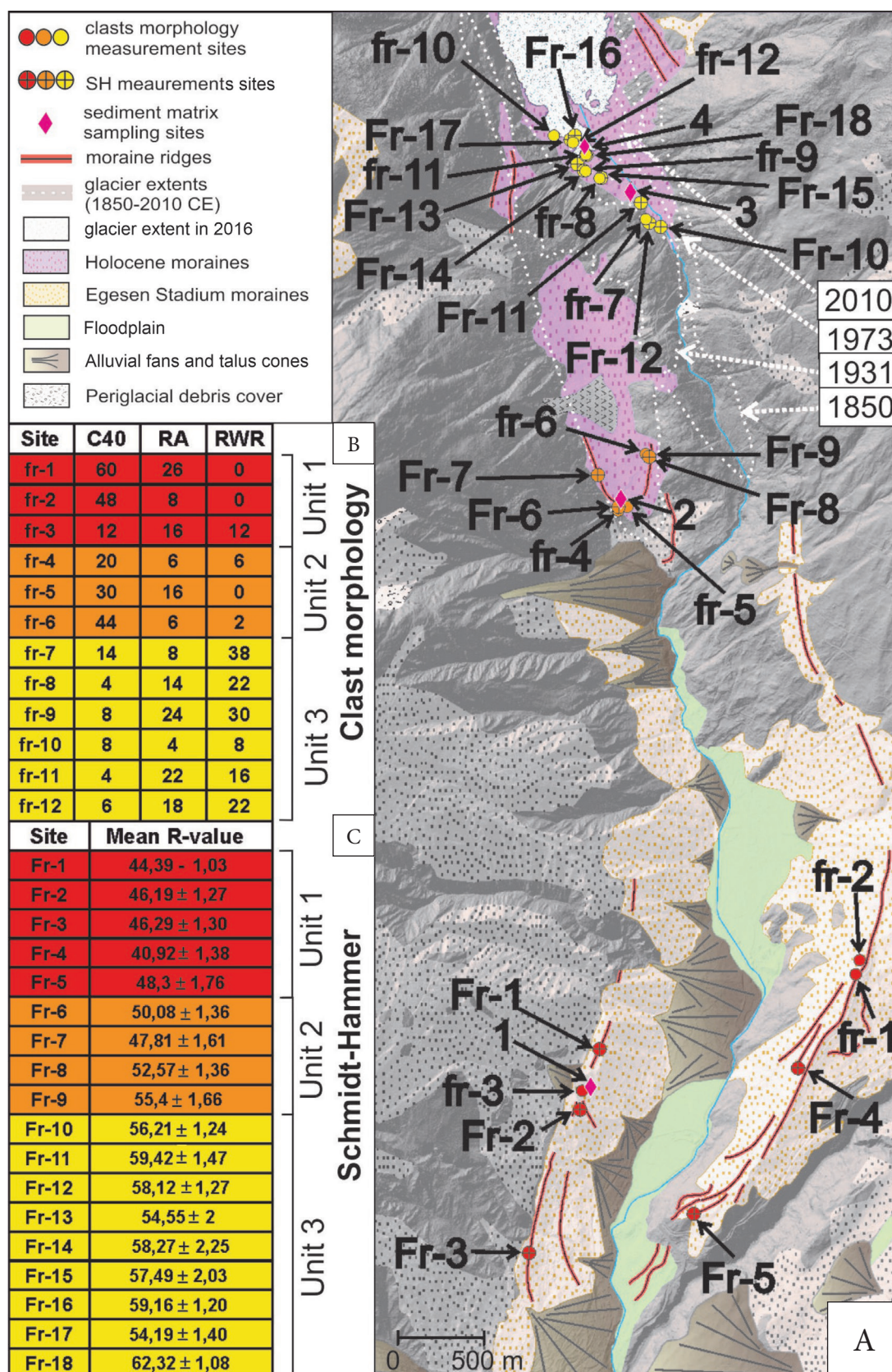
Fig. 2. *Geomorphological map of the Fiescher Valley (A) with the clasts morphology (fr-1-12) (B) and SH weathering sites (Fr-1-18) (C). Single Arabic numbers 1–4 refer to sites where fine-grained sediments were collected*

To support macroscopic observations and compare past and current dynamics of the glacier, sedimentological analyses and automatic microscope scanning were performed for fine-grained sediments (matrix). Four samples were collected (one from each of the four sites marked with numbers 1–4, Fig. 2A) from the shallow (<0.5 m) surface exposures. Sample 1 (unit 1) was taken from landslide within lateral till (fr-3 site, Fig. 3B) and sample 2 (unit 2) from windthrow. These two samples were picked from the places where clasts were collected (Fig. 2A) and reflects moraine material which were not subjected to long lasting slope processes. Samples 3 and 4 (unit 3) were collected from recent proglacial longitudinal bar. Two samples (1–2) were characterized by a high content of organic matter, therefore, before proceeding to microscopic analyses, were burned. The fractional composition of sediments was determined by dry sieving using sieves ranging from 22.6 mm to 0.5 mm. First, the overall weight of the sample was determined, and then individual weights for each fraction in increments of 0.5φ. To illustrate the fractional composition of sediments <0.5 mm a laser diffraction particle size analysis with Mastersizer 3000 was used (Malvern Panalytical n.d.). Additionally, at least 100 quartz grains with a diameter of 0.7–1.0 mm were manually selected from each sample, which were first cleaned of weathered external coatings with 10% HCL acid (Mycielska-Dowgiałło & Woronko 1998), and then subjected to scanning with an automatic microscope Morphology G3. Using built-in algorithms, the following particle parameters were automatically calculated: roundness, convexity, solidity and elongation.

RESULTS

Geomorphological record of moraines in the Fiescher Valley

Moraine unit 1

Three distinct morphostratigraphic moraine systems (units 1–3) were distinguished between the mouth of the Fiescher Valley and the present-day glacier terminus (Fig. 2A). The most extensive moraine system was attributed to the Egesen stadial (Steck 2011), which is the oldest morphostratigraphic unit in the Fiescher Valley (unit 1). Egesen stadial moraines are located in the lower section of the valley at its confluence with the Rhone Valley about 150 m above the valley floor (1,200–1,500 m a.s.l.). It is the largest and most complex moraine system in the study area with the outermost latero-frontal moraine located close to the town of Fiesch in the Rhone Valley and 7 km down-valley from present-day glacier terminus (Figs. 1, 2A). Up to four recessional moraines have been distinguished within the Egesen stadial moraine complex between 1,080 and 1,300 m a.s.l. (Fig. 2A). The best-preserved sequence of individual nested ridges of accretion-mode lateral moraines are preserved on the left side of the valley, where 3–4 m wide ridges reach a height of 10–20 m and with large (2–3 m) perched boulders especially found at Fr-5 site (Fig. 2A).
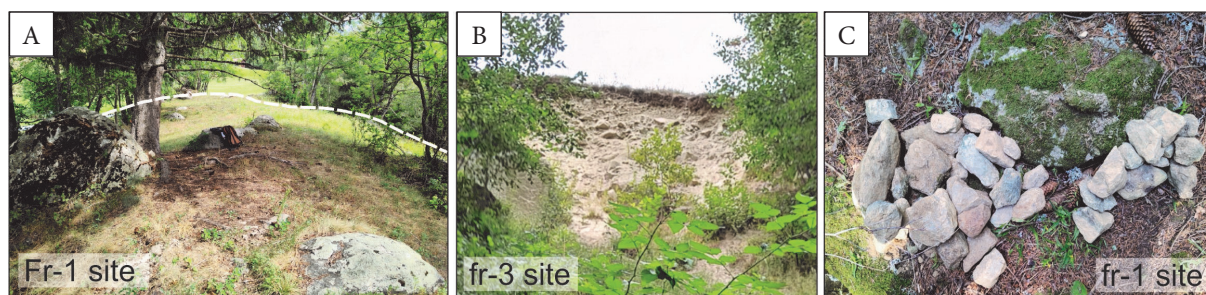

Fig. 3. Landforms and sediments associated with the Egesen stadial in the Fiescher Valley (unit 1). The location of sites is depicted in Figure 2: A) boulder rich right-lateral moraine ridge at Fr-1 site; B) stream-cut exposure in right-lateral moraine at fr-3 site; C) a collection of glacially-transported clast measured at fr-1 site

In contrast, the right-side moraine is poorly preserved and exhibits two sub-ridges partially covered with slope sediments. Larger morainic boulders are found mainly on slopes and within ablation moraine covers in the forested part of the valley (Fig. 3A). The length of the Fiescher Glacier during the Egesen stadial was 20 km.

Moraine unit 2

Upstream, the first unequivocal geomorphological evidence of the younger ice-marginal landforms (unit 2) is found at an elevation of ca. 1,250–1,500 m a.s.l. and ca. 2 km down the valley from the present-day glacier snout (Figs. 2A, 4). The unit 2 moraines were formed by the Neoglacial advances the last time during the LIA (ca. AD 1300–1850/60), with a maximum extent at 1856 CE (Holzhauser 1984). Footprints of mapped ice margins are found only in the western branch of the valley (Fig. 4A, B), while in the rocky bed of the Wysswasser stream, numerous glacial polishes are the only field trace of the glacier activity. The terminal moraines at 1,250 m a.s.l., are relatively poorly preserved and covered by a talus cone (Fig. 2A). Slightly better preserved are recessional latero-frontal moraines at 1,380 m a.s.l. marked on the geological map (Federal Office of Topography Swisstopo 2024a) ca. 200 m up the valley from the maximal LIA extent (Figs. 2A, 4A, B). The 300 m long and 5–10 m high right-side lateral moraine stretches along the western valley side (Fig. 4B, C) while on the eastern side, scattered boulders mark the limit of till drift. Higher up the valley, the presence of lateral moraines has been masked by extensive talus deposits in the valley trough (Figs. 1, 2A). The length of Fiescher Glacier during the LIA was 15 km.
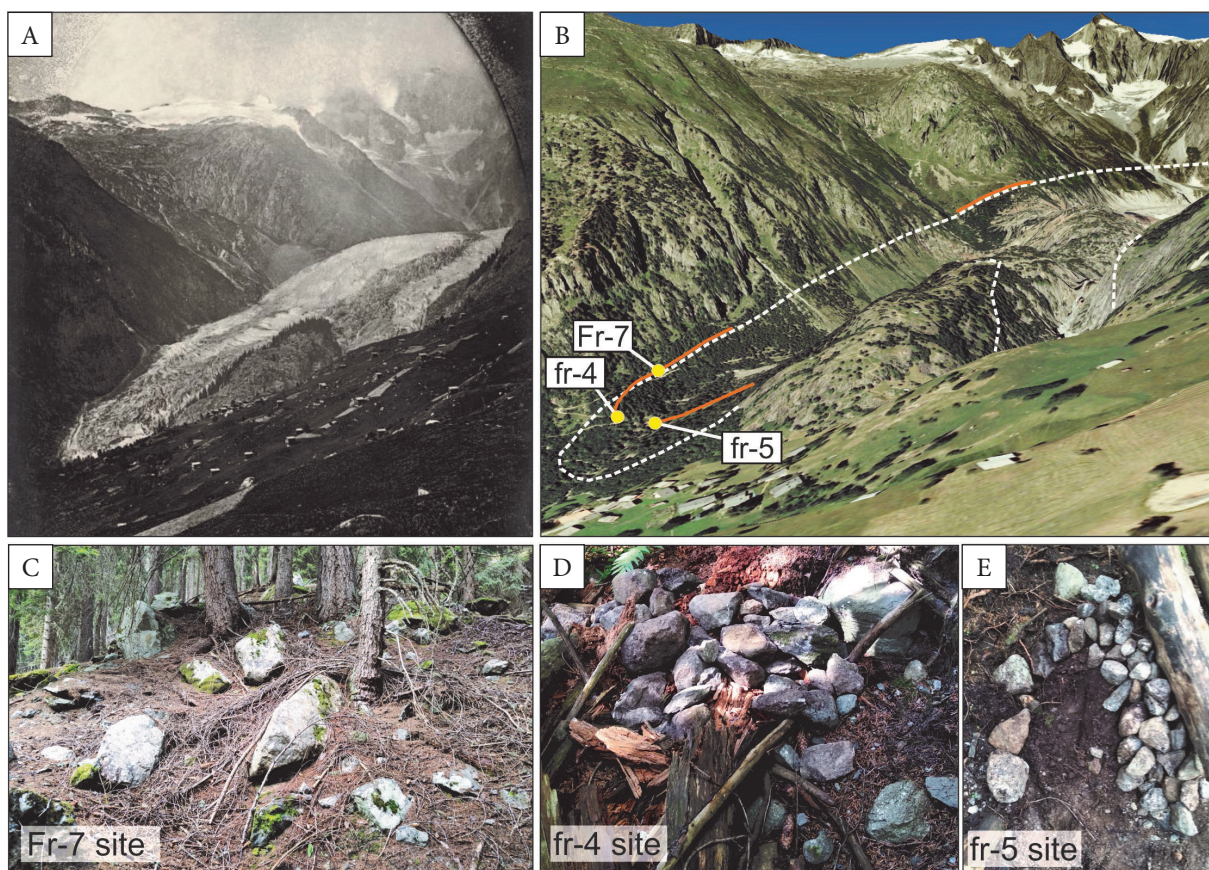

Fig. 4. *Landforms and sediments associated with the Little Ice Age in the Fiescher Valley (unit 2). The location of the sites is depicted in Figure 2: A) Fiescher Glacier extent in 1850 CE (ETH Library's Image Archive n.d.); B) Glacier extent draped over the present-day valley morphology with marked sediment measurement sites (source: Google Earth); C) boulder rich right lateral moraine at Fr-7 site; D) a collection of glacially transported clasts measured at fr-4 site; E) a collection of glacially transported clasts measured at fr-5 site*

The evolution of the moraine complex in the Fiescher Valley (Berner Alps, Switzerland) in the light of Schmidt-hammer...

13

Moraine unit 3

The ice marginal positions marking the Fiescher Glacier front over the last 50 years can be observed in the contemporary glacier forefield, situated between 1,700 and 1,800 m a.s.l. which stretches 700 m down the valley from the present-day glacier terminus. Terminal ice positions in the years 1931, 1973, 2010, and 2016 were determined based on historical photographs (Figs. 1, 2A). The geomorphological evidence of glacier recession is best visible on the western side of the Wysswasser stream, where moraine landforms and sediments were not covered by slope deposits (Fig. 5A). The oldest post-Little Ice Age (LIA) moraines, dated around 1930 CE, were not analyzed due to the difficult access on steep and precipitous ice-moulded slopes. The moraines dating back to the 1973 CE glacier advance form a distinct lateral ridge, standing ca. 5 m above the valley floor (Fr-10 site) (Fig. 5A). This moraine ridge is separated from the glacial polish by a marginal depression. The former glacier front position below the Fr-10 site is indicated by several large boulders resting on bedrock, some of which may have been redeposited from the slope above. The ice margin position in 2010 CE does not exhibit moraine walls. The moraine material is preserved as debris patches resting on bedrock several meters above the present valley floor. The most recent moraine deposits, dating back to 2016 CE, form a discontinuous recessional moraine ridge, standing approximately 5 m high and built with large 1–7 m granite and gneiss boulders (Fig. 5C). On the glacier forefield, the ground moraine sediments are primarily composed of sub- and well-rounded boulders, less than 1 m in size, set within a sandy gravel matrix. These sediments form patches reaching heights of 1.0–1.5 m, which are partially covered by vegetation.
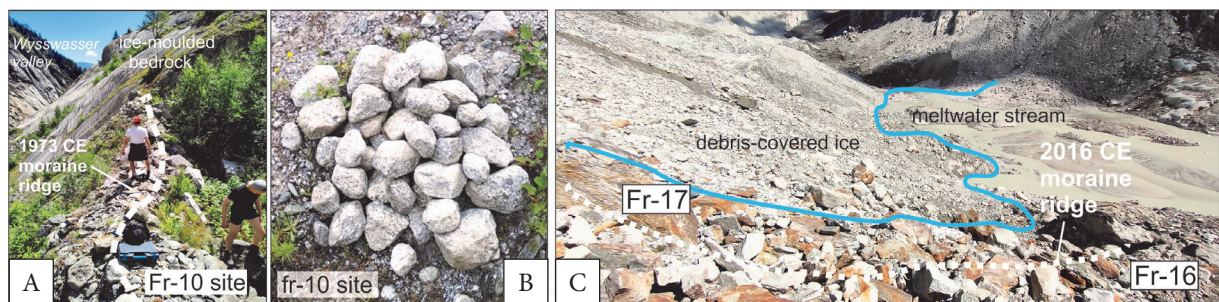

Fig. 5. Sharp-crested right lateral moraine ridge formed during 1973 CE re-advance at Fr-10 site (A); sample of sub-rounded and rounded orthogneiss clasts collected at fr-10 site (B); present-day margin of the Fiescher Glacier with extensive debris cover (blue solid line) and 2016 ice marginal position with marked localization of Fr-16 and Fr-17 SH sites (C)

Schmidt-hammer weathering index and age calibration curve

Schmidt-hammer measurements were obtained from 18 sites, where a total number of 2007 individual measurements were obtained (Table 1). The mean *R*-values range from 40.92 ±1.38 (Fr-4) to 62.32 ±1.08 (Fr-18) (Fig. 2C). The median differs from the mean value usually by less than one point. The exception are sites: Fr-9 (M = 56.75), Fr-11 (M = 61.75), Fr-13 (M = 53.25), Fr-14 (M = 60.25) and Fr-16 (M = 60.25). Except for the Fr-16 site, all listed refer to the results obtained from glacial polishes.

A substantial increase in mean *R*-values may be observed in up valley direction. There is a significant difference between mean *R*-values obtained for three moraine units (Fig. 2C, Table 1). The lowest mean *R*-values (45.06 ±0.6) were obtained for moraine unit 1 which range from 40.92 ±1.38 (Fr-4) to 48.3 ±1.76 (Fr-5). The SH sites located on the ridge of the right lateral moraine (Fr-1, Fr-2, and Fr-3) of the Egesen stadial have similar mean *R*-values and overlapping confidence intervals (Fig. 10). In contrast, the SH sites located on the left side moraines (Fr-4 and Fr-5) are more scattered which may be related to fewer tested boulders.

Table 1
The results of SH measurements in the Fiescher Valley. The location of measurement sites is marked in Figure 2

Stratigraphic unit	SH Site	Morphologic context	Altitude [m a.s.l.]	Lithology	Type and number of measured surfaces	Number of single readings	Overall mean R-value with 95% confidence interval	Overall mean R-value for moraine unit with 95% confidence interval	Overall mean R-value for moraine unit with 95% confidence interval – only for boulder sites
Unit 1	Fr-1	moraine wall, mostly in the forest	1,285–1,290	gneiss	boulder (5)	150	44.39 ±1.03	45.06 ±0.60	45.06 ±0.60
	Fr-2		1,235–1,245	gneiss	boulder (4)	120	46.19 ±1.27		
	Fr-3		1,176	granite	boulder (4)	120	46.29 ±1.30		
	Fr-4		1,265	gneiss	boulder (3)	90	40.92 ±1.38		
	Fr-5		1,171	gneiss	boulder (2)	60	48.3 ±1.76		
Unit 2	Fr-6	moraine wall in the forest	1,370	granite	boulder (5)	150	50.08 ±1.36	51.44 ±0.77	50.34 ±0.84
	Fr-7		1,455	granite	boulder (3)	90	47.81 ±1.61		
	Fr-8		1,447	granite	bulder (4)	120	52.57 ±1.36		
	Fr-9		1,450	gneiss	ice-moulded bedrock (1)	100	55.4 ±1.66		
Unit 3/1973 ce	Fr-10	distinct moraine wall	1,676	orthogneiss, augen gneiss	boulder (5)	150	56.21 ±1.24	57.73 ±0.76	57.17 ±0.89
	Fr-11	ice-moulded bedrock	1,692–1,695	orthogneiss, augen gneiss, amphibolite and migmatite	ice-moulded bedrock (2)	100	59.42 ±1.47		
	Fr-12		1,678	granite, gneiss	boulder (5)	150	58.12 ±1.27		
Unit 3/2010 ce	Fr-13		1,700	migmatite orthogneiss, amphibolite	ice-moulded bedrock (1)	56	54.55 ±2	56.69 ±1.21	–
	Fr-14	ice-moulded bedrock	1690	orthogneiss, augen gneiss	ice-moulded bedrock (1)	50	58.27 ±2.25		
	Fr-15		1,692	orthogneiss, augen gneiss	ice-moulded bedrock (1)	51	57.49 ±2.03		
Unit 3/2016 ce	Fr-16	distinct moraine wall on the glacier forefield	1,690	granite,gneiss	boulder (5)	150	59.16 ±1.20	58.55 ±0.77	58.55 ±0.77
	Fr-17		1,700	gneiss,granite	boulder (5)	150	54.19 ±1.40		
	Fr-18		1,680	granite,gneiss	boulder (5)	150	62.32 ±1.08		

(Combined values spanning Units 3/1973 ce and 3/2010 ce: moraine unit 57.39 ±0.49; boulder sites 58.0 ±0.58)

The *R*-values obtained for the unit 2 moraines are in the range of 47.81 ±1.61 (Fr-7) to 55.4 ±1.66 (Fr-9) with a mean of 51.44 ±0.77. SH results show a statistically significant difference between tested boulders (50.34 ±0.84) and glacial polishes (55.4 ±1.66). The weathering index for the youngest moraine unit 3 is in the wide range from 54.55 ±2 to 62.32 ±1.08 with the overall *R*-value mean of 57.93 ±0.49 (58 ±0.58 for boulders only). Mean *R*-values obtained for boulders and glacial polishes at individual ice-marginal positions (57.73 ±0.76 for 1973 CE, 56.69 ±1.21 for 2010 CE and 58.55 ±0.77 for 2016 CE) do not differ statistically and show overlapping confidence intervals.

Local linear SH age calibration curve and equation used to calculate the exposure time are shown in Figure 6. The rock surface exposure time at the oldest control point (Fr-1) was assumed to be 11.4 ka assuming 2016 moraines as the youngest surface exposed site. The oldest exposure age was achieved for site Fr-4, and it is 13.6 ka ±1.53 ka. Based on results obtained from this curve, we conclude that this curve reflects well the exposure age of glacial deposits in Fiescher Valley. This is confirmed by dates from research in the Berner Alps, according to which the maximum extent of glaciers during the Younger Dryas reached 12–10.7 ka (Ivy-Ochs et al. 2023). In comparison, we tested another variant by setting the oldest control point to 13.2 ka ±1.5 ka and assuming 2016 moraines as the youngest surface exposed site as well. We found that the obtained result, constructed on the basis of site VBA-8 with an age of 13.2 ka, is therefore significantly delayed and cannot be used as a linear age indicator. It refers to a much larger system of the Great Aletsch which corresponds to climate changes with at least several hundred years of delay (Zasadni 2007) hence it cannot be compared with the much smaller Fiescher Glacier.
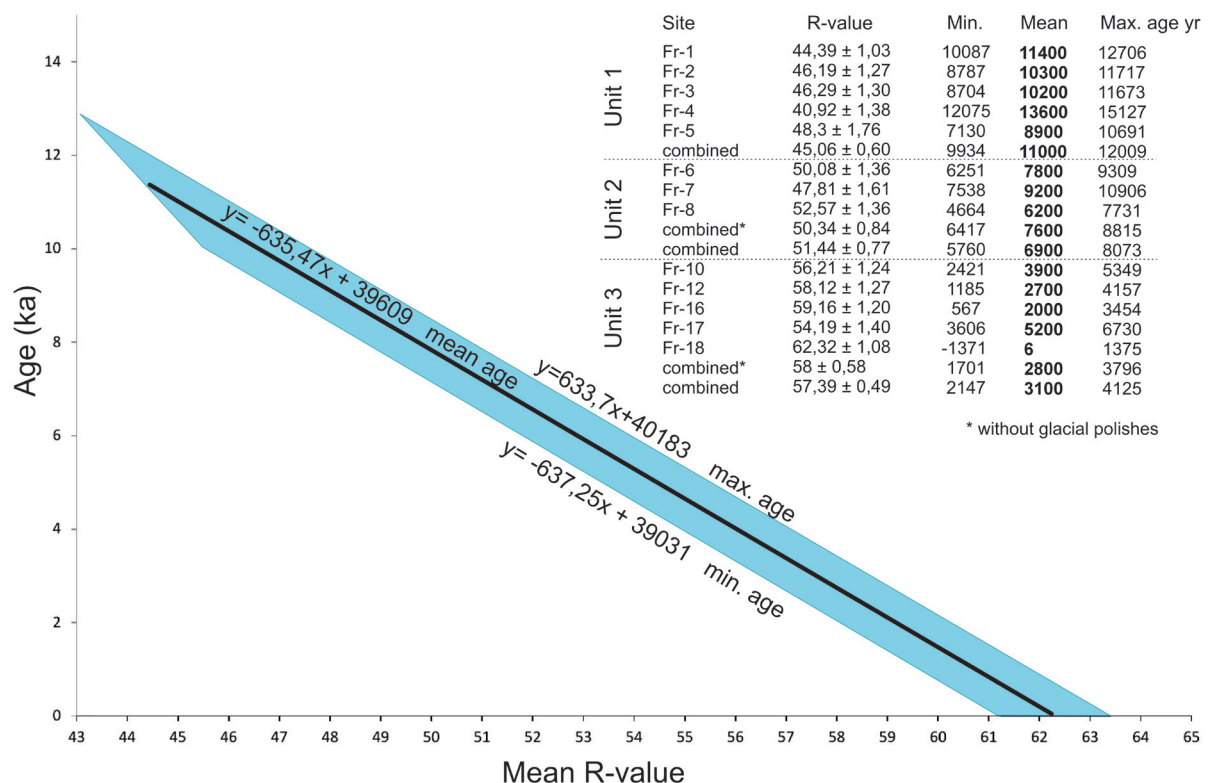

Fig. 6. *Schmidt-hammer exposure dating calibration curve in the Fiescher Valley. Age calibration curve is based on the linear relationship between the average R-values of the youngest (Fr-18) and the oldest (Fr-1) SH sites. Fr-18 site reflects the modern age whereas control age for the Fr-1 site have been adopted according to* ^{10}*Be dates obtained by Schindelwig et al. (2012): 11.4 ka (date from Unnerbäch Glacier). Color bands correspond to the 2-sigma prediction limit (95%) calculated by multiplication of the mean R-values by the main equation. The obtained ages are shown in up right corner and graphically presented in Figure 10*

Additionally, assuming that the oldest preserved moraine ridges in the Fiescher Valley refer to the Egesen stadial (indicated by the entire sequence of moraines and their morphology), their age cannot be older than ca. 13 ka (Ivy-Ochs et al. 2023).

The youngest exposure age (apart from the reference site Fr-18) is characterized by the rock surface sampled at site Fr-16 which is estimated between 2 ka ±1.5 ka.

Clast morphology and fractional analysis

The C_{40} index for the oldest unit 1 glacial sediment shows a high proportion of platy and blade-shaped clasts, while the roundness parameters (RA = 17, RWR = 4) reflect the predominance of sub-rounded (ca. 22%) and subangular (57%) clasts (Figs. 3C, 7). The result of sediment matrix analysis (Fig. 8A) shows the dominance of gravel fraction (55%) which reaches the largest proportion in the study area. The unit 1 moraine sediments are characterized by the smallest circularity (0.733), solidity (0.946) and convexity (0.929)

parameters, while the elongation index is rather high and reaches the value of 0.259 (Fig. 8B). A very strong positive correlation (>0.7) in all samples characterizes the circularity index from convexity and circularity from solidity. A strong (>0.5) or very strong positive correlation characterizes the convexity index from solidity, while a strong negative correlation at sites 3 and 4 characterizes the circularity index from elongation.

A large proportion of platy clasts characterizes the moraine sediments of unit 2 (Fig. 4D, E). The C_{40} index ranges 20–44%, with a mean of 31.3% (Fig. 7). The roundness parameters (RA = 9.3 and RWR = 2.7) are slightly lower than for unit 1 moraines. The fractional composition is similar to unit 1 moraines, with slightly greater dominance of the sand fraction (32%) and a smaller share of the gravel fraction (46%) (Fig. 8A). However, the analysis of quartz grains showed different textural features compared to the oldest sediments (Fig. 8B). The elongation index (0.225) is the smallest among all samples, while circularity (0.806) and solidity (0.963) indexes are the highest.
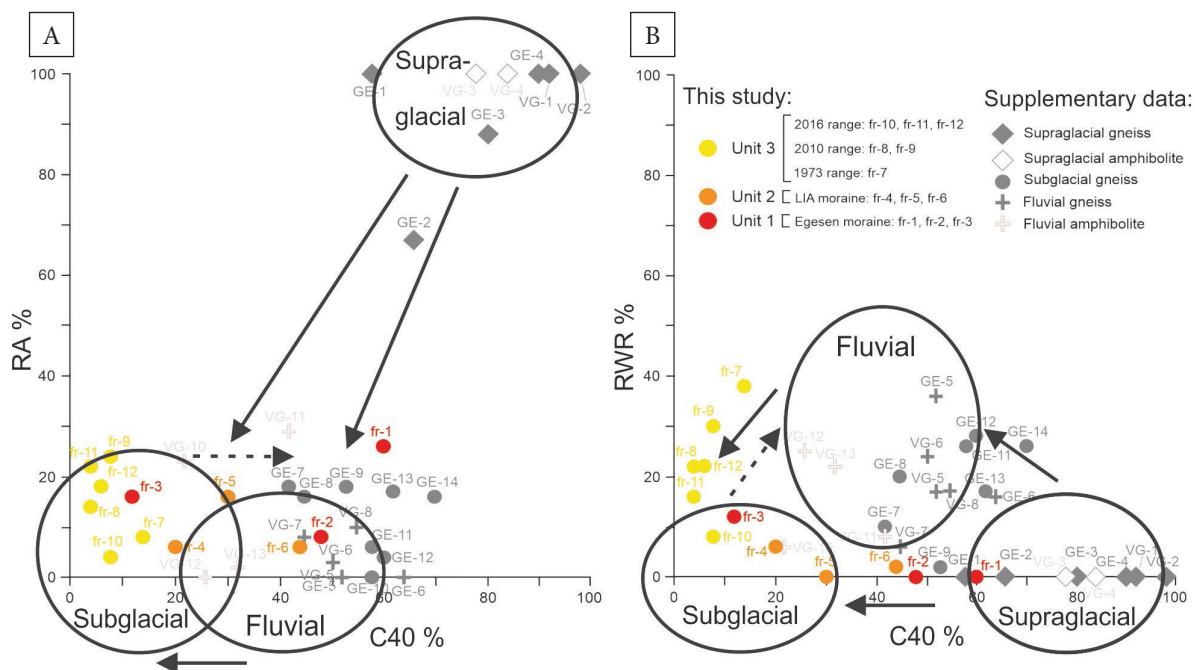

Fig. 7. *Results of clast shape and roundness analysis plotted against the typical transport pathways in glaciated catchments built with massive crystalline lithology (Lukas et al. 2013). The location of the sites is depicted in Figure 2: A) co-variance plot of the RA-index against the C_{40} index; B) co-variance plot of the RWR index against the C_{40} index. Supplementary data adopted from Lukas et al. 2013*
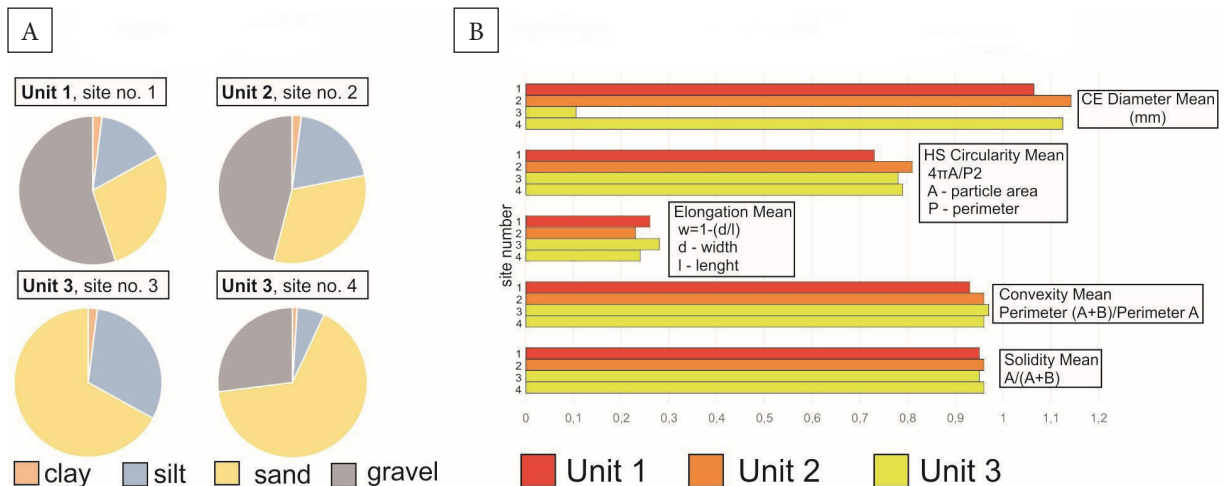
Fig. 8. *Results of sedimentological analysis of fine-grained (matrix) deposits in the Fiescher Valley. The location of the sites is depicted in Figure 2: A) granulometric composition of studied sites; B) morphometric parameters of quartz grains obtained from Morphology G3 analysis*

Clast shape analysis for unit 3 moraines shows the lowest proportion of platy clasts and domination of isometric (blocky) shapes (Figs. 5B, 7). The mean C_{40} index values for individual ice-marginal positions are 14% for 1973 CE moraines and 6% for both 2010 and 2016 CE sites. The low C_{40} index strongly corresponds with the high RWR index, which reaches its highest value in the study area, indicating a greater proportion of rounded and well-rounded clasts (Fig. 7). Nevertheless, the relatively high proportion of very angular and angular clasts (14–24%) suggests the importance of subglacial transport path (Fig. 7). The composition of fine-grained sediments shows a large proportion of sand fraction (66–67% at site 4) (Fig. 8A). The highest proportion of silt fraction was found at site 3 (31%) whereas the gravel fraction share at site 4 amounted to 27%, indicating the good sorting of sediment on the glacier forefield. This implies that bed load competency declines relatively quickly, over hundreds of meters on the glacier forefield. Perhaps the relatively high silt content at site 3 indicates the existence, at least periodically, of pools of standing water which can be attributed to periods after flood episodes. Quartz grains at site 3 are characterized by the highest elongation (0.277) and convexity (0.966) indexes together with a high circularity index (0.79 at site 4 and 0.78 at site 3) (Fig. 8B).

DISCUSSION

A clast transport pathway in the glaciated environment of the Fiescher Valley

The geomorphological analysis, supported by the clasts morphology and grain size analysis, supplies insights into the history and processes of moraine formation of the fourth largest valley glacier in the Alps. The analyzed sediments in the Fiescher Valley are linked to glacier-derived sediments (actively transported sediment) as is visible by the large proportion of subrounded and subangular clasts (73%). In all of the studied sediment sites, the percentage of very angular and angular clasts does not exceed 30%. The initial platy morphology (C_{40} indices = 60) and predominantly very angular and angular shape (1% and 11%, respectively) of massive type gneisses and granitoids were substantially reduced during glacier transport. However, the dependence of clast form and roundness with distance and sediment age is hardly visible. The higher platiness (C_{40} = 48–60%) features the oldest unit 1 moraine located ca 7 km down the valley from the present-day glacial snout (Figs. 1, 2). The presence of high C_{40} and low RWR values clasts suggests passive transportation which is close to the typical values for supraglacially transported debris (Fig. 7) (Lukas et al. 2013).

This is also indicated by the morphometric parameters of the quartz grains which reach the lowest values of circularity and convexity parameters (Fig. 8B). The large production of supraglacial debris during Egesen stadial is well recognised by the distinct, sharp-crested and notably blocky latero-frontal moraines (Ivy-Ochs et al. 2022). On the other hand, lateral moraines could have also contained much more passively transported debris from rockfalls than moraines located closer to the valley axis, where actively transported material predominates (Benn & Balantyne 1994). These actively transported clasts have been eroded and thus supraglacial debris of the latero-frontal moraine of the Egesen stadial is preserved along valley sides as an erosional relict. The highest C_{40} found in the study area could also be related to the frost weathering during the Younger Dryas cold period when the Egesen moraines were impacted by the activity of periglacial processes (Buchenauer 1990, Ivy-Ochs et al. 2022).

The C_{40}/RWR covariance analysis for unit 2 moraines shows the sedimentological signature of subglacially transported debris (Fig. 7). The lowest C_{40} and the highest RWR values (15–40%) were found for the youngest moraine unit, highlighting significant subglacial reworking processes at the recently exposed glacier forefield. A similar clast morphology was observed on recently exposed glacier forefields in the Austrian Alps (Le Heron et al. 2021), where small annual moraines are dominated by sub-rounded to rounded pebble to cobble-sized clasts. It can be linked with position of the sites of unit 3 in the axis of the valley where actively transported material dominates. The high content of sand fraction in fine-grained deposits (Fig. 8) together with high RWR values (Fig. 7) suggests that subglacial sediment contains sand and gravels resulting from glaciofluvial processes. We cannot rule out the possibility that the downwash process occurring during the infiltration of soil particles decreased the number of finer fractions at sites 1 and 2. However, it is not manifested well by the granulometry diagrams (Fig. 8A). Our data suggest that at the present-day glacier foreland supraglacial transported debris could be mixed with strongly reworked subglacial and fluvioglacial clasts. The competing influence

of subglacial and proglacial are typical features of contemporary Alpine glacial depositional systems (Avian et al. 2018).

The clast morphology data obtained enable us to reconstruct the debris cascade in the strongly glaciated valley built with massive crystalline rocks. We found that glacial sediments in the Fiescher Valley show a typical signature of clast reworking in the area built with low-anisotropy (massive) lithology, where debris glacial transport is dominated by subglacial erosion and transportation pathways (Boulton 1978, Lukas et al 2013). In such an environment platiness (C_{40} index) and angularity/roundness (RWR) are good discriminators between glacial and nonglacial sediments. Supraglacial sediments are characterized by high C_{40} (60–100%), high RA (80–100%) and very low RWR (0%) (Fig. 7) (Lukas et al. 2013). In contrast, subglacial sediments feature low C_{40} (0–30%), low RA (0–20%) and low RWR (0–10%) (Fig. 7) (Lukas et al. 2013). A significant reworking and progressive clast edge-rounding of glacial sediments transported clasts found in the study area resulted from glacial erosion and transportation mechanisms. These processes led to a decrease in platiness (as indicated by the reduction in C_{40}, see Fig. 7) and the formation of stable, blocky clast forms.

Schmidt-hammer exposure ages of moraines and their implications for the deglaciation process

The calibration of the Schmidt-hammer *R*-values with surfaces of known age was originally developed in Scandinavia (Shakesby et al. 2006, 2011, Matthews & Owen 2010, Mattthews & Winkler 2011, Matthews & Wilson 2015) and New Zeland (Winkler 2005, 2009) and was further applied to date the glacial features in the British Isles (Tomkins et al. 2016), Pyrenees (Tomkins et al. 2018b), Tatra Mountains (Zasadni et al. 2020) and Karkonosze Mountains (Engel et al. 2011). The SHED has also been recently applied in Alpine geomorphological studies as a method for reconstruction of the post-LGM and post-LIA glacier fluctuations (Scapozza 2012, Scotti et al. 2017, Longhi & Guglielmin 2020, 2021, Scapozza et al. 2021) and currently (post-LIA) ongoing weathering process (Dąbski et al. 2023).
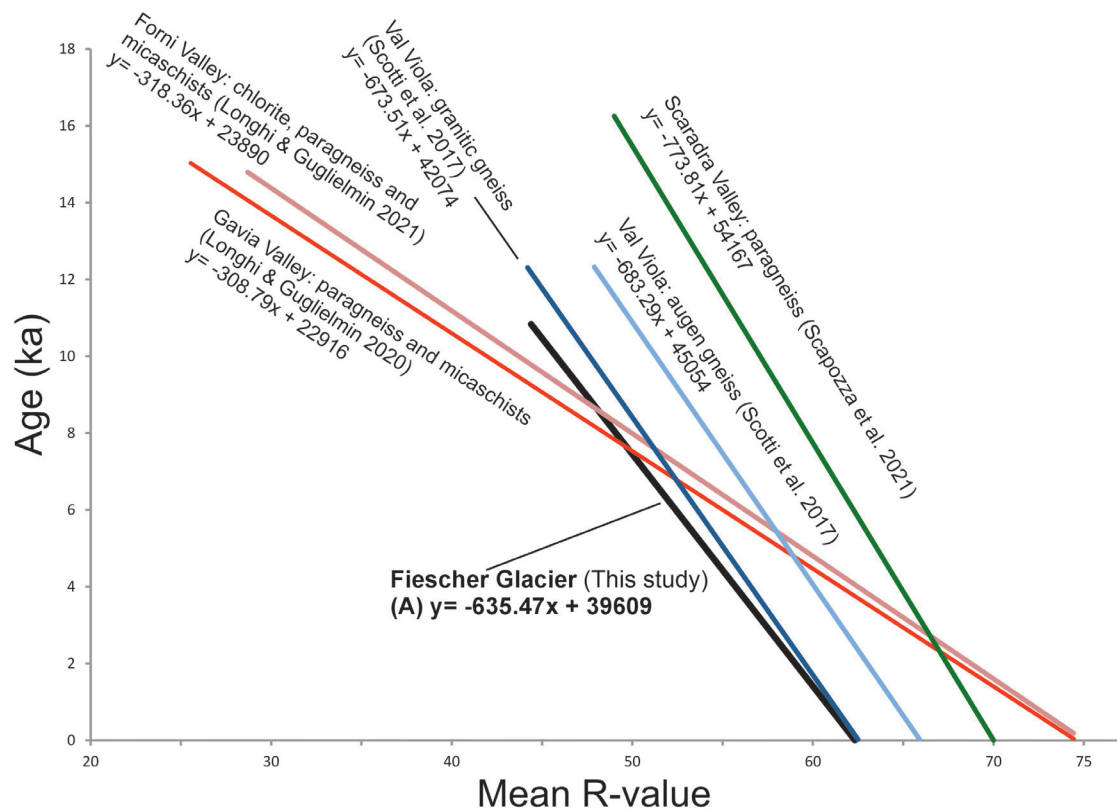
Fig. 9. *Comparison of local linear Schmidt-hammer calibration curves in the Alps. The light blue curve refers to augen gneisses, the dark blue curve refers to granite gneisses sampled in the Val Viola area (Scotti et al. 2017). The green line refers to the extreme values in the Splügenpass area (Scapozza et al. 2021). Red lines mark the extreme values reported in the works of Longhi & Guglielmin (2020, 2021)*

These studies documented that the weathering rate of rock material expressed by the slope of the calibration curves is mainly controlled by different lithological conditions between the studied sites. Foliated metamorphic rocks such as paragneisses and mica schists produce a much gentler slope of the calibration curve (Longhi & Guglielmin 2020, 2021) when compared to massive crystalline rocks (Scotti et al. 2017, Scapozza et al. 2021) (Fig. 9). The new Schmidt-hammer calibration curve for the Fiescher Valley obtained on massive granites and gneisses (Figs. 6, 9) shows a similar statistical regression as the one presented by Scotti et al. (2017) for granitic gneisses in the Val Viola valley.

The Schmidt-hammer relative age categories for moraine units in the Fiescher Valley are in the correct stratigraphic order, featuring a progressive increase in mean *R*-values in an up valley direction. The lowest mean *R*-value covering a range from 40.92 and 48.3 was obtained for unit 1 moraines

(Fr 1-5 sites, Fig. 2). The calculated age of the mean *R*-value for this unit (45.06 ±0.6) is between 12.0 ka and 9.9 ka (Fig. 9) and could be roughly associated with Egesen stadial, corresponding to the glacier advance during the Younger Dryas (12.9–11.5 ka) (Steck 2011) and Early Holocene standstill phases. However, the wide range of SH exposure ages obtained points to the complex evolution of the unit 1 moraine system which was built as a result of several glacial advances marked by up to five moraines (Fig.1). The oldest exposure age ca. 12.9 ka. was obtained at Fr-4 site and may thus be correlated with the oldest glacial advance during the Egesen I stadial (Scotti et al. 2017). The exposure age of the Fr-1 boulders overlaps with Fr-4 site and falls into the YD/Holocene period. The age of these boulders could be correlated with phases III and IV in the Gavia Valley (Longhi & Guglielmin 2020) or phase II in the Forni Valley (Longhi & Guglielmin 2021) (Fig. 10).
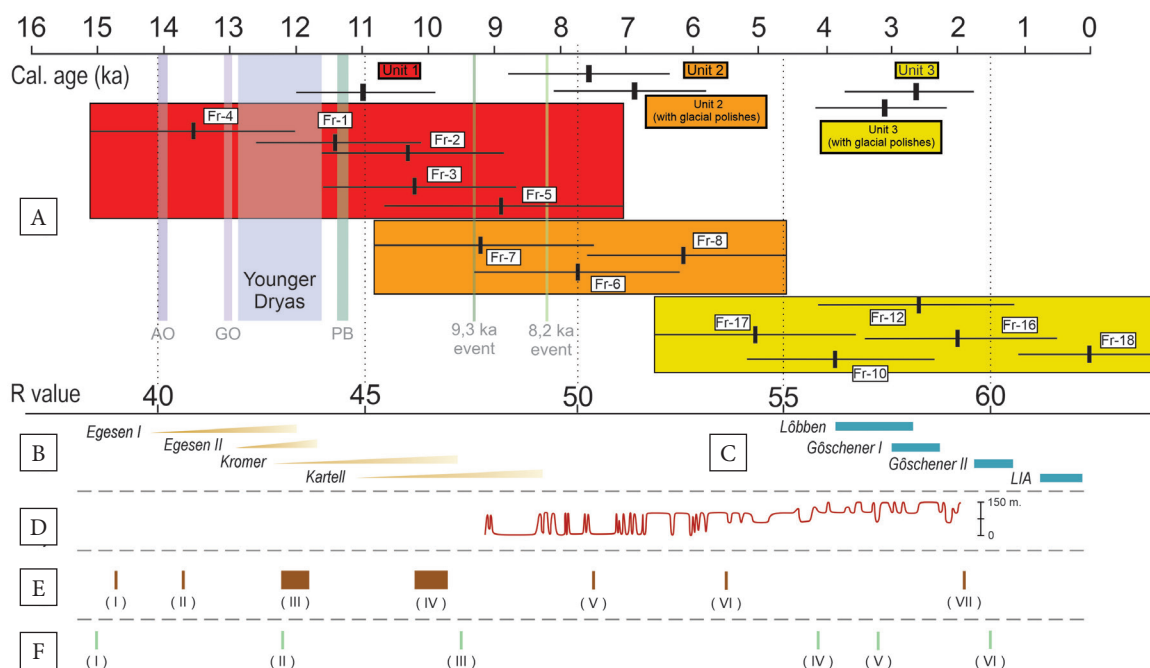
AO - Aegelsee Oscillation (Older Dryas); GO - Gerzensee Oscillation; PB - Preboreal Oscillation; the '9.3 ka event' and the '8.2 ka event' (Misox cold phase) - after Schindelwig et al., 2012

Fig. 10. *Results of SH measurements compiled with climatic and glaciological data reported from the Alps: R-value range grouped into morphostratigraphical units and set against calibrated time scale (A); glacial stages distinguished by Scotti et al. (2017) (B); cold neoglacial oscillations after Zasadni (2007) (C); changes in the thickness of the Upper Grindelwald Glacier based on the records in speleothems in the Milchbach Cave (Luetscher et al. 2011), the value of 0 refers to the altitude of 1750 m a.s.l. (D); glacial phases in the Central Italian Alps given by Longhi & Guglielmin (2020, 2021) (E, F)*

The younger exposure ages falling into 10.2–10.3 ka calculated for Fr-2 and Fr-3 sites, respectively point to Fiescher Glacier moraine formation close to maximal Egesen stadial position also during the Early Holocene. The obtained SHED ages for the Fr-2 and Fr-3 sites fall into phase IV distinguished in Gavia Valley (Longhi & Guglielmin 2020). These standstill phases occurred after 10.5 ka (Ivy-Ochs et al. 2009, Solomina et al. 2015) and were described by Braumann et al. (2020) as a Central European Cold Phase (CE-1, ca. 10 ka), and correspond to the Kartell glacial phase. A similar age of moraine stabilization at 9.9 ka ±0.7 ka, was obtained in Ochsental (Eastern European Alps) (Braumann et al. 2020). It should therefore be considered that during the Early Holocene the Fiescher Glacier was close (1.0–1.5 km) to its maximal extent during the Egesen stadial (Figs. 1, 2). The data provide evidence of the

multiphase glacier readvances of the Fischer glacier during the Younger Dryas and Early Holocene.

The linear calibration for *R*-values measured for the glacial surfaces in the up-valley part of the Fiescher Valley did not provide results consistent with the assumed glacier history of the area. The calculated age of the mean *R*-value for unit 2 is slightly diversified between boulders (8.8–6.4 ka) and glacial polishes (8.0–5.7 ka). The obtained exposure ages are clearly too old assuming the LIA age (approx. 1850 CE) of this moraine (Fig. 4). The lack of young boulders within sampled moraine could be linked with: (1) incorporation of older, more weathered boulders from glacial forefield by push mechanism of moraine formation (Matthews and Shakesby 1984) during the LIA advance, (2) relatively clean glacier snout during the LIA advance that caused little debris incorporation within unit 2 moraines. This hypothesis is

not supported, however, by archival photos (ETH Library's Image Archive) which rather confirm the presence of a 'dirty' snout during the LIA advance. The relatively old debris within unit 2 moraines could have originated from earlier glacier activity in this area and closely related failure process (rockfalls). The overall SHED age of unit 2 falls into cold Misox oscillation (8.4–7.3 ka), which was identified in pollen analyses in Ticino, Switzerland (Zoller 1958, Ivy-Ochs et al. 2009) and with phase V glacial presented by Longhi and Guglielmin (2020). At the same time in the Berner Alps advances of the Upper Grindelwald glacier have been documented between 9.2–2.0 ka (Luetscher et al. 2011, Fig. 10). According to Solomina et al. (2015) short glacier advances were documented in the Alps during the period 6.8–7.7 ka. Hence, the Schmidt-hammer data suggest that the most likely previously formed Middle Holocene moraines were overridden by the much more extensive LIA advance and material mixed during the glacier advance.

Similarly, the obtained SHED ages for the youngest post-Little Ice Age (LIA) moraines (unit 3) are much older than the expected age of moraine formation (Fig. 9). The age of the mean R-value for this unit (58 ±0.58) is between 1.7 and 3.7 ka (Fig. 9) thus nearly 2 ka older than expected age of moraine formation. The highest R-values (ca. 70) were only obtained for one site (Fr-18) located at contemporary moraines and represented a fresh surface without weathering. This age discrepancy could be linked to the presence of extensive supraglacial moraine cover at the present-day glacier snout (Fig. 5) containing more weathered rockfall debris of much older exposure age (Kellerer-Pirklbauer 2008, Matthews & Winkler 2022). This indicates that the currently retreating glacier snout is experiencing substantial extraglacial debris production, leading to a significant disparity in the exposure ages of boulders depending on the time of moraine formation. Surprisingly, few examples of the application of SHED to Late Holocene (Neoglacial) moraines exist in the literature and are limited to small, relatively clean glaciers in Scandinavia and the Alps. The SHED data acquired in this study suggest that the occurrence of "too old" boulders might be a prevalent characteristic of Holocene moraines, owing to their intricate evolutionary history which should be taken into account during any chronological interpretation.

CONCLUSIONS

Geomorphological mapping, combined with the results of Schmidt-hammer dating, confirm that the Fiescher Valley was continuously occupied by a valley-type glacier during the Late Glacial and Holocene. Three distinct morphostratigraphic moraine systems (moraine units) were distinguished: the most extensive and the oldest Egesen stadial moraines, Neoglacial moraines reaching a maximum extent in 1850 CE, and the most recent recessional moraines within the range of the glacier extents in 1973, 2010 and 2016 CE. A large proportion of clasts with subrounded and subangular classes point to substantial reworking by subglacial erosion and transport. Clast morphology show a typical signature of clast reworking in the alpine areas built with low-anisotropy (massive) lithology. In such an environment, the platiness (C_{40} index) and angularity/roundness (RWR) are good discriminators between glacial and nonglacial sediments. The trend of rock surface weathering in the Fiescher Valley is comparable with the Central Italian Alps (Scotti et al. 2017) and the Lepontine Alps (Scapozza et al. 2021) built with similar massive crystalline rocks. Distinguished moraine units are independent episodes of glacier advances which is confirmed by SH dating as well as clast shape analysis. The calculated age of the oldest moraine unit is between 12.0–9.9 ka and could be associated with the Egesen stadial, corresponding to the glacier advance during the Younger Dryas (12.9–11.5 ka) and Early Holocene standstill phases. In contrast, SHED ages obtained for the LIA and the most recent moraines are much older than the assumed glacier advances. Assuming a linear relationship between the age and R-values, the presence of much older boulders found on LIA ice limits may result from the incorporation of older, more weathered boulders from the glacial forefield by the prominent LIA advance. Another possibility is a nonlinear relationship between the age and R-values. The most recent glacier advances are associated with the formation of extensive supraglacial moraine cover containing

more weathered rock-fall debris of a much older exposure age and mixed with strongly reworked subglacial and fluvioglacial deposits. This potential age discrepancy should be taken into account in its chronological interpretation of moraines in large, glaciated valley systems.

REFERENCES

Avian M., Kellerer-Pirklbauer A. & Lieb G.K., 2018. Geomorphic consequences of rapid deglaciation at Pasterze Glacier, Hohe Tauern Range, Austria, between 2010 and 2013 based on repeated terrestrial laser scanning data. *Geomorphology*, 310, 1–14. https://doi.org/10.1016/j.geomorph.2018.02.003.

Ballantyne C.K., 1982. Aggregate clast form characteristics of deposits near the margins of four glaciers in the Jotunheimen Massif, Norway. *Norsk Geografisk Tidsskrift – Norwegian Journal of Geography*, 36(2), 103–113. https://doi.org/10.1080/00291958208621960.

Baroni C., Gennaro S., Salvatore M.C., Ivy-Ochs S., Christl M., Cerrato R. & Orombelli G., 2021. Last Lateglacial glacier advance in the Gran Paradiso Group reveals relatively drier climatic conditions established in the Western Alps since at least the Younger Dryas. *Quaternary Science Reviews*, 255, 106815. https://doi.org/10.1016/j.quascirev.2021.106815.

Benn D.I. & Ballantyne C.K., 1994. Reconstructing the transport history of glacigenic sediments: a new approach based on the co-variance of clast form indices. *Sedimentary Geology*, 91(1–4), 215–227. https://doi.org/10.1016/0037-0738(94)90130-9.

Benn D.I., Kirkbride M.P., Owen L.A. & Brazier V., 2003. Glaciated valley landsystems. [in:] Evans D.J.A. (ed.), *Glacial Landsystems*, Arnold, London, 372–406.

Böhlert R., Egli M., Maisch M., Brandová D., Ivy-Ochs S., Kubik P.W. & Haeberli W., 2011. Application of a combination of dating techniques to reconstruct the Lateglacial and early Holocene landscape history of the Albula region (eastern Switzerland). *Geomorphology*, 127(1–2), 1–13. https://doi.org/10.1016/j.geomorph.2010.10.034.

Boulton G.S., 1978. Boulder shapes and grain-size distributions of debris as indicators of transport paths through a glacier and till genesis. *Sedimentology*, 25(6), 773–799. https://doi.org/10.1111/j.1365-3091.1978.tb00329.x.

Braumann S.M., Schaefer J.M., Neuhuber S.M., Reitne J.M., Lüthgens Ch. & Fiebig M., 2020. Holocene glacier change in the Silvretta Massif (Austrian Alps) constrained by a new ^{10}Be chronology, historical records and modern observations. *Quaternary Science Reviews*, 245, 106493. https://doi.org/10.1016/j.quascirev.2020.106493.

Buchenauer H.W., 1990. *Gletscher- und Blockgletschergeschichte der westlichen Schobergruppe (Osttirol)*. Marburger Geographische Schriften, 117, Selbstverlag der Marburger Geographischen Gesellschaft, Marburg/Lahn.

Dąbski M., Badura I., Kycko M., Grabarczyk A., Matlakowska R. & Otto J.Ch., 2023. The development of limestone weathering rind in a proglacial environment of the Hallstätter Glacier. *Minerals*, 13(4), 530. https://doi.org/10.3390/min13040530.

Engel Z., Traczyk A., Braucher R., Woronko B. & Křížek M., 2011. Use of ^{10}Be exposure ages and Schmidt hammer data for correlation of moraines in the Krkonoše Mountains, Poland/Czech Republic. *Zeitschrift für Geomorphologie*, 55(2), 175–196. https://doi.org/10.1127/0372-8854/2011/0055-0036.

ETH Library's Image Archive E-Pics, n.d. https://ba.e-pics.ethz.ch/# [access: 11.03.2024].

Federal Office for Meteorology and Climatology MeteoSwiss, n.d. www.meteoswiss.admin.ch [access: 24.01.2024].

Federal Office of Topography Swisstopo, 2024a. *Geological Atlas of Switzerland 1:25,000*. https://www.swisstopo.admin.ch/en/geological-atlas-of-switzerland-1-25000 [access: 24.01.2024].

Federal Office of Topography Swisstopo, 2024b. *National Map 1:25'000*. https://www.swisstopo.admin.ch/en/national-map-1-25000 [access: 24.01.2024].

Federal Office of Topography Swisstopo, 2024c. *swiss ALTI3D* [the high precision digital elevation model of Switzerland]. https://www.swisstopo.admin.ch/en/height-model-swissalti3d [access: 24.01.2024].

Glacier Monitoring in Switzerland (GLAMOS), n.d. www.glamos.ch/en/#inventories/A55f-03 [access: 24.01.2024].

Goodsell B., Hambrey M.J. & Glasser N.F., 2005. Debris transport in a temperate valley glacier: Haut Glacier d'Arolla, Valais, Switzerland. *Journal of Glaciology*, 51(172), 139–146. https://doi.org/10.3189/172756505781829647.

Goudie A.S., 2006. The Schmidt Hammer in geomorphological research. *Progress in Physical Geography*, 30(6), 703–718. https://doi.org/10.1177/0309133306071954.

Gross G., Kerschner H. & Patzelt G., 1977. Methodische Untersuchungen über die Schneegrenze in alpinen Gletschergebieten. *Zeitschrift* für *Gletscherkunde und Glazialgeologie*, 12(2), 223–251.

Hambrey M., Glasser N., & Goodsell B., 2002. Formation of band ogives and associated structures at Bas Glacier d'Arolla, Valais, Switzerland. *Journal of Glaciology*, 48(161), 287–300. https://doi.org/10.3189/172756502781831494.

Holzhauser H., 1984. *Zur Geschichte der Aletschgletscher und des Fieschergletschers*. Physiche Geographie, 13, University of Zürich, Department of Geography, Zürich, Switzerland.

Hormes A., Müller B.U. & Schlüchter Ch., 2001. The Alps with little ice: evidence for eight Holocene phases of reduced glacier extent in the Central Swiss Alps. *The Holocene*, 11(3), 255–265. https://doi.org/10.1191/095968301675275728.

Ivy-Ochs S., 2015. Glacier variations in the European Alps at the end of the last glaciation. *Cuadernos de Investigación Geográfica: Geographical Research Letters*, 41(2), 295–315. https://doi.org/10.18172/cig.2750.

Ivy-Ochs S., Schlüchter C., Kubik P.W., Synal H.A., Beer J. & Kerschner H., 1996. The exposure age of an Egesen moraine at Julier Pass, Switzerland measured with the cosmogenic radionuclides Be-10, Al-26 and Cl-36. *Eclogae Geologicae Helvetiae*, 89, 1049–1063. https://doi.org/10.48350/87205.

Ivy-Ochs S., Kerschner H., Reuther A., Maisch M., Sailer R., Schaefer J., Kubik P.W., Synal H.A. & Schlüchter C., 2006. The timing of glacier advances in the northern European Alps based on surface exposure dating with cosmogenic ^{10}Be, ^{26}Al, ^{36}Cl, and ^{21}Ne. [in:] Siame L.L., Bourlès D.L., Brown E.T. (eds.), *In Situ-Produced Cosmogenic Nuclides and Quantification of Geological Processes*, Geological Society of America Special Paper, 415, Geological Society of America, Boulder, Colorado, 43–60. https://doi.org/10.1130/2006.2415(04).

Ivy-Ochs S., Kerschner H., Maisch M., Christl M., Kubik P.W. & Schlüchter C., 2009. Latest Pleistocene and Holocene glacier variations in the European Alps. *Quaternary Science Reviews*, 28(21–22), 2137–2149. https://doi.org/10.1016/j.quascirev.2009.03.009.

Ivy-Ochs S., Monegato G. & Reitner J.M., 2022. Chapter 58 – The Alps: glacial landforms from the Last Glacial Maximum. [in:] Palacios D., Hughes P.D., García-Ruiz J.M. & de Andrés N. (eds.), *European Glacial Landscapes: Maximum Extent of Glaciations*, Elsevier, 449–460. https://doi.org/10.1016/B978-0-12-823498-3.00030-3.

Ivy-Ochs S., Monegato G. & Reitner J.M., 2023. The Alps: glacial landforms from the Younger Dryas Stadial. [in:] Palacios D., Hughes P.D., García-Ruiz J.M. & de Andrés N. (eds.), *European Glacial Landscapes: Last Deglaciation*, Elsevier, 525–539. https://doi.org/10.1016/B978-0-323-91899-2.00058-9.

Joerin U.E., Stocker T.F. & Schlüchter C., 2006. Multicentury glacier fluctuations in the Swiss Alps during the Holocene. *The Holocene*, 16(5), 697–704. https://doi.org/10.1191/0959683606hl964rp.

Kellerer-Pirklbauer A., 2008. The Schmidt Hammer as a relative age dating tool for rock glacier surfaces: examples from Northern and Central Europe. [in:] Kane D.L. & Hinkel K.M. (eds.), *Ninth International Conference on Permafrost. Volume 1*, Institute of Northern Engineering, University of Alaska, Fairbanks, 913–918.

Kelly M.A., Kubik P.W., Von Blanckenburg F. & Schlüchter C., 2004. Surface exposure dating of the Great Aletsch Glacier Egesen moraine system, western Swiss Alps, using the cosmogenic nuclide ^{10}Be. *Journal of Quaternary Science*, 19(5), 431–441. https://doi.org/10.1002/jqs.854.

Kirkbride M.P. & Winkler S., 2012. Correlation of Late Quaternary moraines: Impact of climate variability, glacier response, and chronological resolution. *Quaternary Science Reviews*, 46, 1–29. https://doi.org/10.1016/j.quascirev.2012.04.002.

Kłapyta P., 2012. Ewolucja rzeźby wysokogórskiej Tatr Zachodnich w późnym glacjale i holocenie. [in:] Borówka R.K., Cedro A. & Kavetskyy I. (red.), *Współczesne problemy badań geograficznych*, PPH ZAPOL Dmochowski, Sobczyk, Szczecin, 73–82.

Kłapyta P., 2013. Application of Schmidt hammer relative age dating to Late Pleistocene moraines and rock glaciers in the Western Tatra Mountains, Slovakia. *CATENA*, 111, 104–121. https://doi.org/10.1016/j.catena.2013.07.004.

Kłapyta P., 2020. Geomorphology of the high-elevated flysch range – Mt. Babia Góra Massif (Western Carpathians). *Journal of Maps*, 16(2), 689–701. https://www.doi.org/10.1080/17445647.2020.1800530.

Kłapyta P., Mîndrescu M. & Zasadni J., 2021. Geomorphological record and equilibrium line altitude of glaciers during the last glacial maximum in the Rodna Mountains (eastern Carpathians). *Quaternary Research*, 100, 1–20. https://doi.org/10.1017/qua.2020.90.

Labhart T.P., 1977. *Aarmassiv und Gotthardmassiv*. Gebrüder Borntraeger, Berlin – Stuttgart.

Le Heron D.P., Kettler Ch., Davies B.J., Scharfenberg L., Eder L., Ketterman M., Griesmeier G.E.U., Quinn R., Chen X., Vandyk T. &. Busfield M.E., 2021. Rapid geomorphological and sedimentological changes at a modern Alpine ice margin: lessons from the Gepatsch Glacier, Tirol, Austria. *Journal of the Geological Society*, 179(3), jgs2021-052. https://doi.org/10.1144/jgs2021-052.

Longhi A. & Guglielmin M., 2020. Reconstruction of the glacial history after the Last Glacial Maximum in the Italian Central Alps using Schmidt's hammer R-values and crystallinity ratio indices of soils. *Quaternary International*, 558, 19–27. https://doi.org/10.1016/j.quaint.2020.08.045.

Longhi A. & Guglielmin M., 2021. The glacial history since the Last Glacial Maximum in the Forni Valley (Italian Central Alps). Reconstruction based on Schmidt's Hammer R-values and crystallinity ratio indices of soils. *Geomorphology*, 387, 107765. https://doi.org/10.1016/j.geomorph.2021.107765.

Luetscher M., Hoffmann D.L., Frisia S. & Spötl C., 2011. Holocene glacier history from alpine speleothems, Milchbach cave, Switzerland. *Earth and Planetary Science Letters*, 302(1–2), 95–106. https://doi.org/10.1016/j.epsl.2010.11.042

Lukas S. & Benn D.I., 2006. Retreat dynamics of Younger Dryas glaciers in the far NW Scottish Highlands reconstructed from moraine sequences. *Scottish Geographical Journal*, 122(4), 308–325. https://doi.org/10.1080/14702540701235142,

Lukas S., Benn D.I., Boston C.M., Brook M., Coray S., Evans D.J., Graf A., Kellerer-Pirklbauer A., Kirkbride M.P., Krabbendam M., Lovell H., Machiedo M., Mills S.C., Nye K., Reinardy B.T.I., Ross F.H. & Signer M., 2013. Clast shape analysis and clast transport paths in glacial environments: A critical review of methods and the role of lithology. *Earth-Science Reviews*, 121, 96–116. https://doi.org/10.1016/j.earscirev.2013.02.005.

Malvern Panalytical, n.d. *Morphologi G3*. https://www.malvernpanalytical.com/en/support/product-support/morphologi-range/morphologi-g3 [access: 24.01.2024].

Matthews J.A. & Owen G., 2010. Schmidt hammer exposure-age dating: developing linear age-calibration curves using Holocene bedrock surfaces from the Jotunheimen–Jostedalsbreen regions of southern Norway. *Boreas*, 39(1), 105–115. https://doi.org/10.1111/j.1502-3885.2009.00107.x.

Matthews J.A. & Shakesby R.A., 1984. The status of the 'Little Ice Age' in southern Norway: relative-age dating of Neoglacial moraines with Schmidt hammer and lichenometry. *Boreas*, 13(3), 333–346. https://doi.org/10.1111/j.1502-3885.1984.tb01128.x

Matthews J.A. & Wilson P., 2015. Improved Schmidt-hammer exposure ages for active and relict pronival ramparts in southern Norway, and their palaeoenvironmental implications. *Geomorphology*, 246, 7–21. https://doi.org/10.1016/j.geomorph.2015.06.002.

Matthews J.A. & Winkler S., 2011. Schmidt-hammer exposure-age dating (SHD): Application to early Holocene moraines and a reappraisal of the reliability of terrestrial cosmogenic-nuclide dating (TCND) at Austanbotnbreen, Jotunheimen, Norway. *Boreas*, 40(2), 256–270. https://doi.org/10.1111/j.1502-3885.2010.00178.x.

Matthews J.A. & Winkler S., 2022. Schmidt-hammer exposure-age dating: A review of principles and practice. *Earth-Science Reviews*, 230, 104038. https://doi.org/10.1016/j.earscirev.2022.104038.

Müller F.B., Caflisch T. & Müller G., 1976. *Firn und Eis der Schweizer Alpen: Gletscherinventar*. Eidgenössische Technische Hochschule, Geographisches Institut, Zürich.

Mycielska-Dowgiałło E. & Woronko B., 1998. Analiza obtoczenia i zmatowienia ziarn kwarcowych frakcji piaszczystej i jej wartość interpretacyjna. *Przegląd Geologiczny*, 46(12), 1275–1281.

Pallàs R., Rodés Á., Braucher R., Bourlès D., Delmas M., Calvet M. & Gunnell Y., 2010. Small, isolated glacial catchments as priority targets for cosmogenic surface exposure dating of Pleistocene climate fluctuations, southeastern Pyrenees. *Geology*, 38(10), 891–894. https://doi.org/10.1130/G31164.1.

Placek A. & Migoń P., 2005. Zastosowanie młotka Schmidta w badaniach geomorfologicznych – potencjał, ograniczenia i wstępne wyniki badań w Sudetach. [in:] Kotarba A., Krzemień K. & Święchowicz J. (red.), *Współczesna ewolucja rzeźby Polski: VII Zjazd Geomorfologów Polskich, Kraków, 19–22 września 2005*, Instytut Geografii i Gospodarki Przestrzennej Uniwersytetu Jagiellońskiego, Kraków, 367–371 .

Powers M.C., 1953. A new roundness scale for sedimentary particles. *Journal of Sedimentary Research*, 23(2), 117–119. https://doi.org/10.1306/D4269567-2B26-11D7-8648000102C1865D.

Reznichenko N.V., Davies T.R.H. & Winkler S., 2016. Revised palaeoclimatic significance of Mueller Glacier moraines, Southern Alps, New Zealand. *Earth Surface Processes and Landforms*, 41(2), 196–207. https://doi.org/10.1002/esp.3848.

Roberson S., 2008. Structural composition and sediment transfer in a composite cirque glacier: Glacier de St. Sorlin, France. *Earth Surface Processes and Landforms*, 33(13), 1931–1947. https://doi.org/10.1002/esp.1635.

Rounce D.R., Hock R., Maussion F., Hugonnet R., Kochtitzky W., Huss M., Berthier E., Brinkerhoff D., Compagno L., Copland L., Farinotti D., Menounos B. & McNabb R.W., 2023. Global glacier change in the 21st century: Every increase in temperature matters. *Science*, 379(6627), 78–83. https://doi.org/10.1126/science.abo1324.

Scapozza C., 2012. *Stratigraphie, morphodynamique, paléoenvironnements des terrains sédimentaires meubles à forte déclivité du domaine périglaciaire alpin*, Géovisions, 40, Université de Lausanne, Lausanne, Suisse.

Scapozza C., Del Siro C., Lambiel C. & Ambrosi C., 2021. Schmidt hammer exposure-age dating of periglacial and glacial landforms in the Southern Swiss Alps based on R-value calibration using historical data. *Geographica Helvetica*, 76(4), 401–423. https://doi.org/10.5194/gh-76-401-2021.

Schimmelpfennig I., Schaefer J., Lamp J., Godard V., Schwartz R., Bard E., Tuna T., Akçar N., Schlüchter C., Zimmerman S. & Aster T., 2021. Glacier response to Holocene warmth inferred from in situ ^{10}Be and ^{14}C bedrock analyses in Steingletscher's forefield (central Swiss Alps). *Climate of the Past*, 18(1), 23–44. https://doi.org/10.5194/cp-18-23-2022.

Schindelwig I., Akçar N., Kubik P.W. & Schlüchter Ch., 2012. Lateglacial and early Holocene dynamics of adjacent valley glaciers in the Western Swiss Alps. *Journal of Quaternary Science*, 27(1), 114–124. https://doi.org/10.1002/jqs.1523.

Scotti R., Brardinoni F., Crosta G.B., Cola G. & Mair V., 2017. Time constraints for post-LGM landscape response to deglaciation in Val Viola, Central Italian Alps. *Quaternary Science Reviews*, 177, 10–33. https://doi.org/10.1016/j.quascirev.2017.10.011.

Shakesby R.A., Matthews J.A. & Owen G., 2006. The Schmidt hammer as a relative-age dating tool and its potential for calibrated-age dating in Holocene glaciated environments. *Quaternary Science Reviews*, 25(21–22), 2846–2867. https://doi.org/10.1016/j.quascirev.2006.07.011.

Shakesby R.A., Matthews J.A., Karlén W. & Los S.O., 2011. The Schmidt hammer as a Holocene calibrated-age dating technique: testing the form of the R-value-age relationship and defining the predicted-age errors. *The Holocene*, 21(4), 615–628. https://doi.org/10.1177/0959683610391322.

Solomina O.N., Bradley R.S., Hodgson D.A., Ivy-Ochs S., Jomelli V., Mackintosh A.N., Nesje A., Owen L.A., Wanner H., Wiles G.C. & Young N.E., 2015. Holocene glacier fluctuations. *Quaternary Science Reviews*, 111, 9–34. https://doi.org/10.1016/j.quascirev.2014.11.018.

Steck A., 2011. *1269 Aletschgletscher mit Teil von 1249 Finsteraarhorn: Erläuterungen*. Geologischer Atlas der Schweiz 1:25 000, 131, Schweizerische Eidgenossenschaft Bundesamt für Landestopografie Swisstopo.

Sumner P. & Nel W., 2002. The effect of rockmoisture on Schmidt hammer rebound: Tests on rock samples from Marion Island and South Africa. *Earth Surface Processes and Landforms*, 27(10), 1137–1142. https://doi.org/10.1002/esp.402.

Tomkins M.D., Dortch J.M. & Hughes P.D., 2016. Schmidt Hammer exposure dating (SHED): Establishment and implications for the retreat of the last British Ice Sheet. *Quaternary Geochronology*, 33, 46–60. https://doi.org/10.1016/j.quageo.2016.02.002.

Tomkins M.D., Huck J.J., Dortch J.M., Hughes P.D., Kirbride M.P. & Barr I.D., 2018a. Schmidt Hammer exposure dating (SHED): Calibration procedures, new exposure age data and an online calculator. *Quaternary Geochronology*, 44, 55–62. https://doi.org/10.1016/j.quageo.2017.12.003.

Tomkins M.D., Dortch J.M., Hughes P.D., Huck J.J., Stimson A.G., Delmas M., Calvet M. & Pallàs R., 2018b. Rapid age assessment of glacial landforms in the Pyrenees using Schmidt hammer exposure dating (SHED). *Quaternary Research*, 90(1), 26–37. https://doi.org/10.1017/qua.2018.12.

Viles H., Goudie A., Grab S. & Lalley J., 2011. The use of the Schmidt Hammer and Equotip for rock hardness assessment in geomorphology and heritage science: A comparative analysis. *Earth Surface Processes and Landforms*, 36(3), 320–333. https://doi.org/10.1002/esp.2040.

Wentworth Ch.K., 1922. A scale of grade and class terms for clastic sediments. *The Journal of Geology*, 30(5), 377–392. http://www.jstor.org/stable/30063207.

Winkler S., 2005. The Schmidt hammer as a relative-age dating technique: potential and limitations of its application on Holocene moraines in Mt Cook National Park, Southern Alps, New Zealand. *New Zealand Journal of Geology and Geophysics*, 48(1), 105–116. https://doi.org/10.1080/00288306.2005.9515102.

Winkler S., 2009. First attempt to combine terrestrial cosmogenic nuclide (10Be) and Schmidt hammer relative-age dating: Strauchon Glacier, Southern Alps, New Zealand. *Central European Journal of Geosciences*, 1(3), 274–290. https://doi.org/10.2478/v10085-009-0026-3.

Winkler S., Matthews J.A., Haselberger S., Hill J.L., Mourne R.W., Owen G. & Wilson P., 2020. Schmidt-hammer exposure-age dating (SHD) of sorted stripes on Juvflye, Jotunheimen (central South Norway): Morpho-dynamic and palaeoclimatic implications. *Geomorphology*, 353, 107014. https://doi.org/10.1016/j.geomorph.2019.107014.

Zasadni J., 2007. The Little Ice Age in the Alps: its record in glacial deposits and rock glacier formation. *Studia Geomorphologica Carpatho-Balcanica*, 41, 117–131.

Zasadni J. & Kłapyta P., 2016. From valley to marginal glaciation in alpine-type relief: Lateglacial glacier advances in the Pięć Stawów Polskich/Roztoka Valley, High Tatra Mountains, Poland. *Geomorphology*, 253, 406–424. https://doi.org/10.1016/j.geomorph.2015.10.032.

Zasadni J., Kłapyta P., Broś E., Ivy-Ochs S., Świąder A., Christl M. & Balážovičová L., 2020. Latest Pleistocene glacier advances and post-Younger Dryas rock glacier stabilization in the Mt. Kriváň group, High Tatra Mountains, Slovakia. *Geomorphology*, 358, 107093. https://doi.org/10.1016/j.geomorph.2020.107093.

Zingg T., 1935. *Beitrag zur Schotteranalyse*. Eidgenössische Technische Hochschule in Zürich, Zürich [PhD thesis].

Zoller H., 1958. Pollenanalytische Untersuchungen im unteren Misox mit den ersten Radiokarbondatierungen in der Südschweiz. *Veröffentlichungen des Geobotanischen Institutes Rübel in Zürich*, 34, 166–175.